Geochronology, Petrogenesis and Tectonic Setting of the Late Triassic syenite porphyry from the Western Part of the North Qinling Orogenic Belt

Shuqin Li , Zuochen Li * , Xianzhi Pei , Hao Lin , Li Qin , Shang Ji , Yajie Yang , Jinghong Ren

Posted Date: 10 November 2023

doi: 10.20944/preprints202311.0705.v1

Keywords: North Qinling orogen belt; Late Triassic; tectonic setting; petrogenesis; geochronology; syenitic porphyries

Article

Geochronology, Petrogenesis and Tectonic Setting of the Late Triassic syenite porphyry from the Western Part of the North Qinling Orogenic Belt

Shuqin Li [1], Zuochen Li [1,2,*], Xianzhi Pei [1,2], Hao Lin [1], Li Qin [1], Shang Ji [1], Yajie Yang [1] and Jinghong Ren [1]

[1] Key Laboratory of Western China's Mineral Resources and Geological Engineering, Ministry of Education, School of Earth Science and Resources, Chang'an University, Xi'an 710054, Shaanxi, China
[2] Xi'an Key Laboratory for Mineralization and Efficient Utilization of Critical Metals, Xi'an 710054, Shaanxi, China
* Correspondence: lizuochen@chd.edu.cn

Abstract: Precise determination of the tectonothermal events at the Qinling-Qilian junction is extremely significant for understanding the tectonic evolution of the eastern branch of the Paleo-Tethys. The Banpo porphyry outcrops in the northern margin of the North Qinling were chosen as the research subject, and their formation and tectonic environment were investigated using Zircon U-Pb age geochronology and geochemical studies. The results indicated the final stage of the Triassic orogeny and the closure phase of the Paleo-Tethys. The weighted average values of $^{206}Pb/^{238}U$ ages of samples from 3 sites of the Banpo porphyry corresponded to 213.4 ±2.1 Ma (MSWD = 0.56), 213.0 ±1.6 Ma (MSWD = 0.92), and 213.2 ±4.4 Ma (MSWD = 1.6). The porphyry bodies with high SiO_2 and high alkali is typical A-type granite, which belongs to the weak peraluminous shoshonite series. All the samples are rich in light rare earth elements, exhibiting a seagull-type right-leaning partitioning curve, with an obviously negative Eu anomalies . In addition, based on the regional geological data, it can be concluded that the Banpo porphyry was formed during the transition period from a post-orogenic environment to a non-orogenic environment. This study indicated the closure of the Paleo-Tethys-Mianxian-Lveyang Ocean by the Late Triassic as well as the completion of the collision between the North China and Yangtze Blocks along the Qinling orogenic belt.

Keywords: north qinling orogen belt; late triassic; tectonic setting; petrogenesis; geochronology; syenitic porphyries

1. Introduction

The conjunction area between Qinling and Qilian orogenic belt is the key section of the east-west connection of the central orogenic belt of China, which is located at the intersection of the Tethyan tectonic domain and the Paleo-Asian tectonic domain. It serves as a convergence junction of several blocks and the orogenic belt [1–6]. The Qinling orogenic belt of the Indosinian age exhibits strong magmatic activity, resulting in the formation of volcano plutonic rocks, especially the Indosinian granite, diorite, and other intermediate-acid rocks [7]. These magmatic events not only serve as important records of complex subduction-collision orogeny in the Mesozoic era [6,8–10] but also characterize the deep dynamic mechanism and provide significant insights into the geological structure evolution of the Central China orogenic belt [9,11,12]. Moreover, they are closely associated with the opening and closing processes of the Mianxian-Lueyang Ocean [13–15].

The early and late phases of the Indosinian period are characterized by varying distribution and spreading of the major intrusive rocks formed during those phases. The early intrusive rocks are located in the central and western parts of the southern region of the North Qinling orogenic belt and show a north-south reverse-strip distribution, which is consistent with the regional tectonic lines. The late Indosinian intrusive rocks are primarily distributed in the central south part of the North Qinling orogenic belt, [8,9,16–23]. In recent years, several researchers have studied the Indosinian intrusive

 doi:10.20944/preprints202311.0705.v1

rocks found in the western region of the North Qinling belt and proposed different perspectives on the formation of the tectonic environment, which can be categorized into the early subduction stage and late collision-post-collision stage [2,24–33].

The genesis of granitic rocks, especially A-type granites, is essential for understanding the tectonic formation and evolution of the continental crust. It also provides a novel concept for examining the underlying genetic mechanism and deep dynamic background of collision-type magmatic rocks in the orogenic belt [34–44]. This study has chosen the syenite porphyry outcrops in the western section of the North Qinling orogenic belt to determine its formation age and evaluate its significance in the geological evolution of the western section of the North Qinling orogenic belt through detailed field investigation, geochronology, petrology, and geochemical studies. The results show that Banpo porphyry was formed during the transition period from a post-orogenic environment to a non-orogenic environment, and the closure of the Paleo-Tethys-Mianxian-Lveyang Ocean by the Late Triassic as well as the completion of the collision between the North China and Yangtze Blocks along the Qinling orogenic belt.

2. Geological Background

The Qinling orogenic belt is a composite continental collision orogenic belt composed of two major suture zones, namely, Shangdan and Mianlue, and three blocks, namely, the southern margin of the North China Block, the Qinling micro-block and the northern margin of the Yangtze Block [45]. The western Banpo syenite porphyry of the North Qinling orogenic belt is located along the Boyang-Banpo-vineyard line on the north side of the Weihe River fault to the east of Beidao District, and is uniformly distributed from east to west (Figure 1). To the south, the Qinling Group is connected with both the Paleoproterozoic Qinling Group and the Huluhe Group metamorphosed clastic rock series of the Neopaleozoic. Among these, the Qinling Group is a set of medium-deep metamorphic complexes composed primarily of gneiss, granitic rock, marble, and amphibolite. These have undergone complex tectonic deformation and qualitative action and are characterized by the development of high amphibolite facies. The Huluhe Group is mainly composed of metamorphic clastic rock. The Banpo syenite porphyry intrudes into the Xiaohezi volcanic rocks and the southern part of the intrusion is affected by subsequent faults [17]. Certain mafic microgranular enclaves can also be observed within the porphyry body, with a particle size of approximately 10–15 cm.

Preprints (www.preprints.org) | NOT PEER-REVIEWED | Posted: 10 November 2023 doi:10.20944/preprints202311.0705.v1

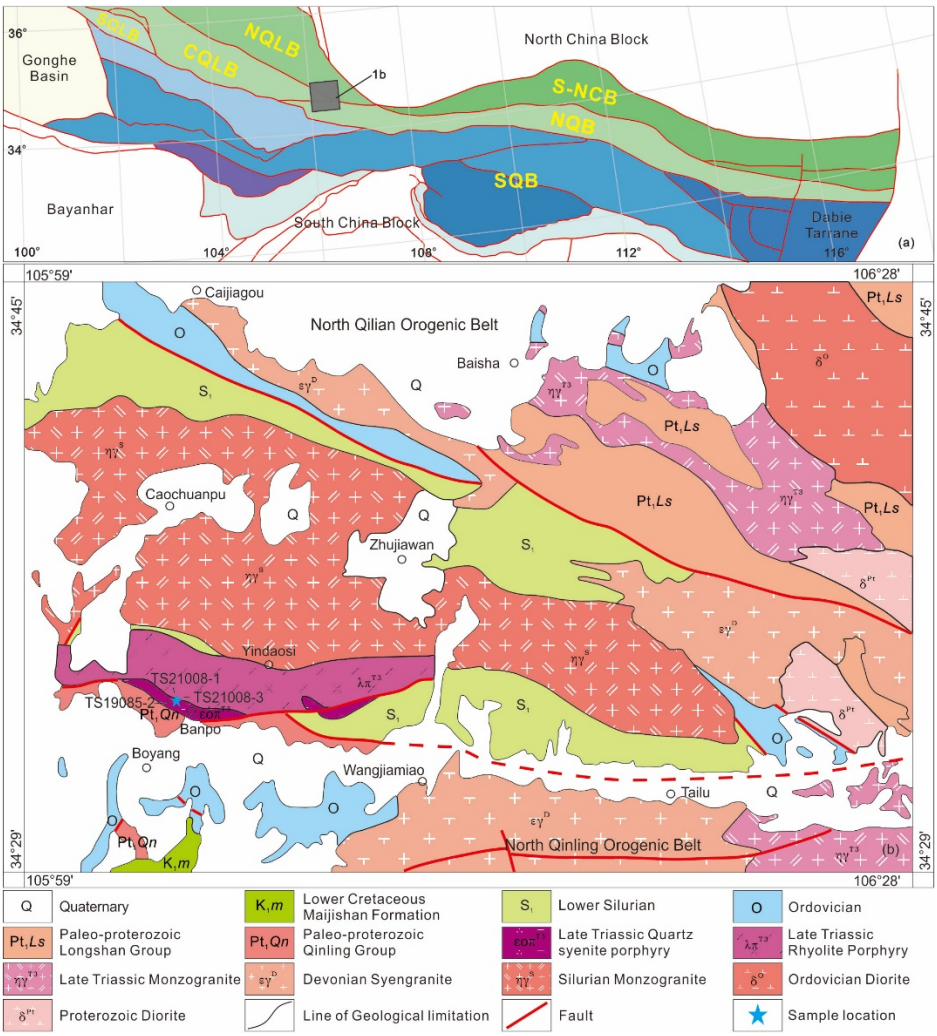

Figure 1. (**a**) Map showing the regional context of the North Qinling Orogenic Belt (WQOB). Geological map modified from Dong et al. [6]; (**b**) Banpo syenite porphyry from Xu et al. [46].

3. Petrography

Syenite porphyry is a dark brick red and porphyritic structure (Figure 2a, b). The phenocrysts are mainly composed of orthoclase and a small amount of plagioclase. Orthoclase contains hemidiomorphic-idiomorphic shaped crystals that are developed into both Carlsbad and lattice twin crystals, which are characterized by long columns and plates (approximately 0.6–1.0 cm long). Its content ranges from about 15–30%, with the range of maximum varying between 35–40%. The groundmass is primarily composed of plagioclase, quartz, and a small amount of potassium feldspar, biotite, magnetite, sphene, and zircon. The orthoclase is hypidiomorphic, with a grain size of 0.07 mm × 0.22 mm to 0.1 mm × 0.3 mm, with 50–60% content, developed into simple twin crystals and visible stripe structures. Potassium feldspar forms a ring-shaped structure around quartz (Figure 2c). The matrix plagioclase can be characterized as polysynthetic twin crystals (Figure 2d), with a 5–10% content. Some of them also have porphyritic structure, massive structure, and are composed of porphyritic and matrix, and the matrix and porphyritic components are mainly composed of plagioclase, potassium feldspar, a small amount of biotite, amphibole and so on. The matrix has microcrystalline structure and cryptocrystalline structure. When there is a small amount of quartz in the porphyry and matrix, it is called quartz monzonite porphyry.

Preprints (www.preprints.org) | NOT PEER-REVIEWED | Posted: 10 November 2023 doi:10.20944/preprints202311.0705.v1

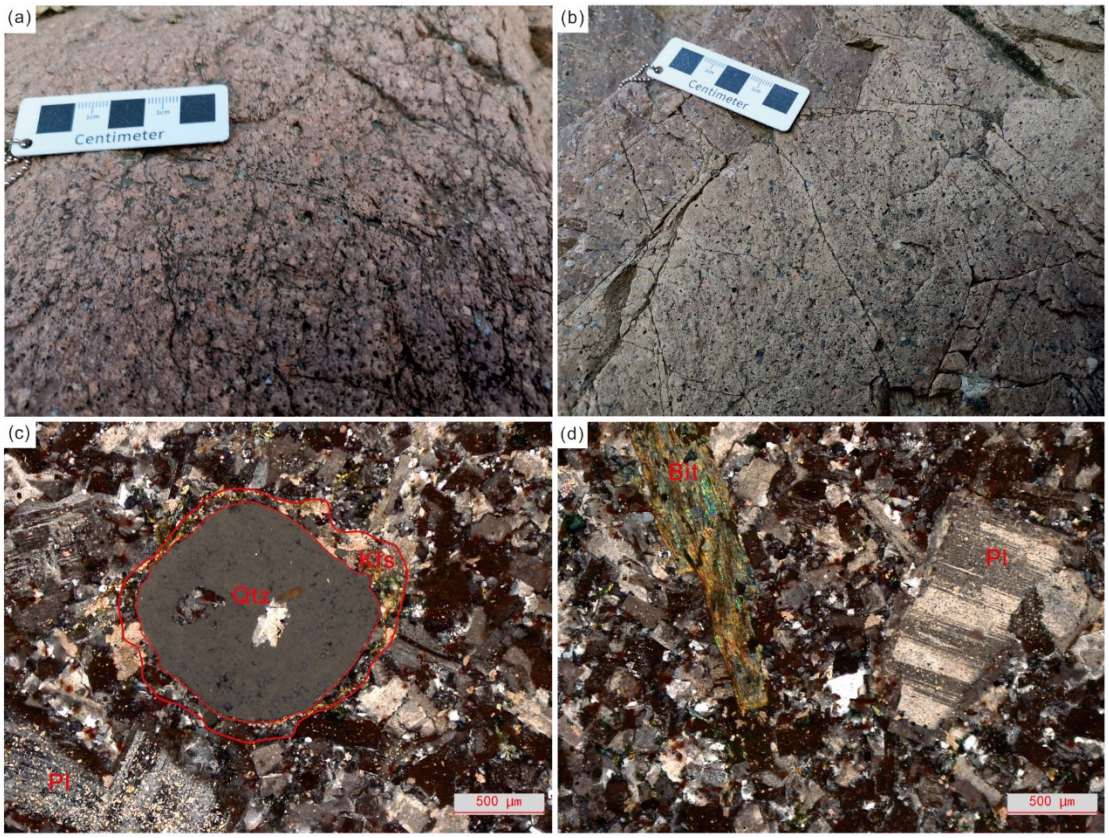

Figure 2. Field photographs and photomicrographs of the Banpo pluton in the west section of North Qinling Orogenic Belt (WNQOB). **(a,b)**field photographs of the Banpo syenite porphyry;(**c,d**) photomicrographs of the Banpo syenite porphyry. Mineral abbreviations are as follows: Qtz = quartz, Pl = plagioclase, Bit = biotite.

4. Analytical Methods

4.1. Zircon U-Pb Geochronology

The geographic coordinates of the samples collected from the syenite porphyry for zircon U-Pb age analysis are 34°33′47′′N, 106°03′56′′E (TS21008–1), 34°33′50′′N, 106°03′57′′E (TS21008–3), and 34°33'43''N, 106°03'55''E (TS19085–2). The samples were crushed and sorted. Subsequently, the transparent zircon grains with no visible inclusions or cracks were examined under a binocular and mounted in epoxy resin. After polishing, the microscopic structure analysis of transreflectance and cathodoluminescence (CL) images was carried out, and the optimal zircon domain for U-Pb isotope dating was selected. The zircon-separated work reported in this study was carried out at Xi'an Ruishi Geological Technology Co., Ltd. The zircon targets and cathodoluminescence (CL) images were provided by Beijing Geoanalysis Co., Ltd. Zircon U-Pb isotope analysis was performed using laser ablation multi-collector inductively coupled plasma mass spectrometry (LA-MC-ICP MS) at Beijing Geoanalysis Co., Ltd. Laser denudation system is GeoLas 2005, ICP-MS is Agilent 7500a. Helium was used as carrier gas, the laser beam spot diameter was 32μm, the denudation depth was 20-40μm, and the laser pulse was 8 Hz. The international standard zircon sample 91500 was used as the external standard sample, the element content was NIST SRM610 as the external standard and Si as the internal standard element. Detailed parameters are shown in Liu et al. [47]. Offline processing of analytical data is completed by using software ICPMSDataCal [48]. The standard zircon GJ-1 was used as the calibration standard for instrument U and Pb isotope fractionation correction. Data reduction harmonic plot preparation, and weighted age calculation were performed using the ICPMS Data Cal8.3 program of Liu et al. [49] and the Isoplot (Version 3.76) program of Ludwig et al. [50]. The ^{208}Pb correction method was employed for correcting common Pb content in zircon samples. The

Preprints (www.preprints.org) | NOT PEER-REVIEWED | Posted: 10 November 2023 doi:10.20944/preprints202311.0705.v1

NIST SRM610 glass standard was used as the external standard. Further details on the analytical method and instrument parameters are specified in Li et al. [49–51].

4.2. Geochemical Analyses

The analysis of major and trace elements of the whole rock was performed in the laboratory of Langfang Fengzeyuan Rock and Mineral Detection Technology Co., Ltd. All samples were broken to less than 200 mesh. The main element test was performed by wavelength dispersive ray fluorescence spectrometer (XRF), and the analysis error was analyzed. For details, see Ma et al. [52].For major element analysis, the sample was initially determined for loss on ignition and then melted into glass sheets. The analytical accuracy of the Shimadzu 1800 X-ray fluorescence spectrometer was around 2%. For the trace element analysis process, 500 mg of sample powder was placed in a Teflon cup. Subsequently, 1.0 mL of pure HF and 1.5 mL of pure HNO_3 were added. The sample was dissolved in the solution by heating at 190 °C for 48 h. Thermo-X7 type ICP-MS was used to analyze the composition of trace elements. The standards BE-N and WS-E were used to monitor instrument stability and the accuracy of trace element analysis was around 10%.

5. Results of Analyses

The zircon U-Pb isotope data and whole-rock geochemistry for the Keri rhyolites are listed in Supplementary Tables S1–S3.

5.1. Zircon U-Pb Age and REE Geochemistry

The zircons of Banpo syenite porphyry are colorless and transparent, with grain sizes between ~100 and 200 μm. The crystals have columnar and long columnar shapes and develop into magmatic crystallization belts. The CL images and measurement points of some typical zircons are shown in Figure 3 [53–55].

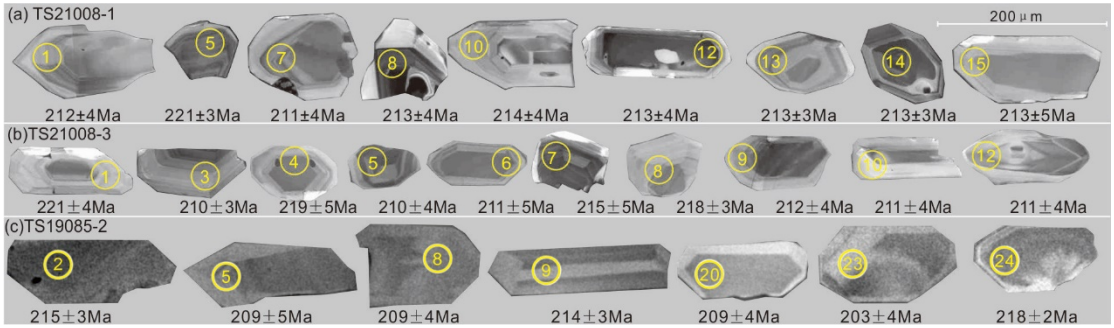

Figure 3. (**a-c**) CL images and single-zircon $^{206}Pb/^{238}U$ ages of zircons.

The Th content of TS21008–1 zircon ranged from 66.99ppm to 547.76ppm, whereas the U content ranged from 90.37ppm to 926.55ppm. The Th/U ratio ranged from 0.38 to 0.98, and the majority of the Th/U ratios exceeded 0.4 (Figure 4a) and the Th and U are positively correlated (Figure 4b). The distribution pattern of rare earth elements demonstrates a left-leaning curve of heavy rare earth enrichment with negative Eu and positive Ce anomalies (Figure 4 g) (Supplementary Table S1). U-Pb isotope age analysis was performed on 25 zircons sampled from Banpo syenite porphyry, and 25 points were determined (Supplementary Table S2). Excluding nine data values with harmonicity less than 90% and significantly higher age values, the remaining $^{206}Pb/^{238}U$ age values ranged from 205 to 221 Ma. The weighted average age of $^{206}Pb/^{238}U$ corresponds to 213.4 ±2.1 Ma, with MSWD = 0.56 (Figure 5a, b).

Preprints (www.preprints.org) | NOT PEER-REVIEWED | Posted: 10 November 2023 doi:10.20944/preprints202311.0705.v1

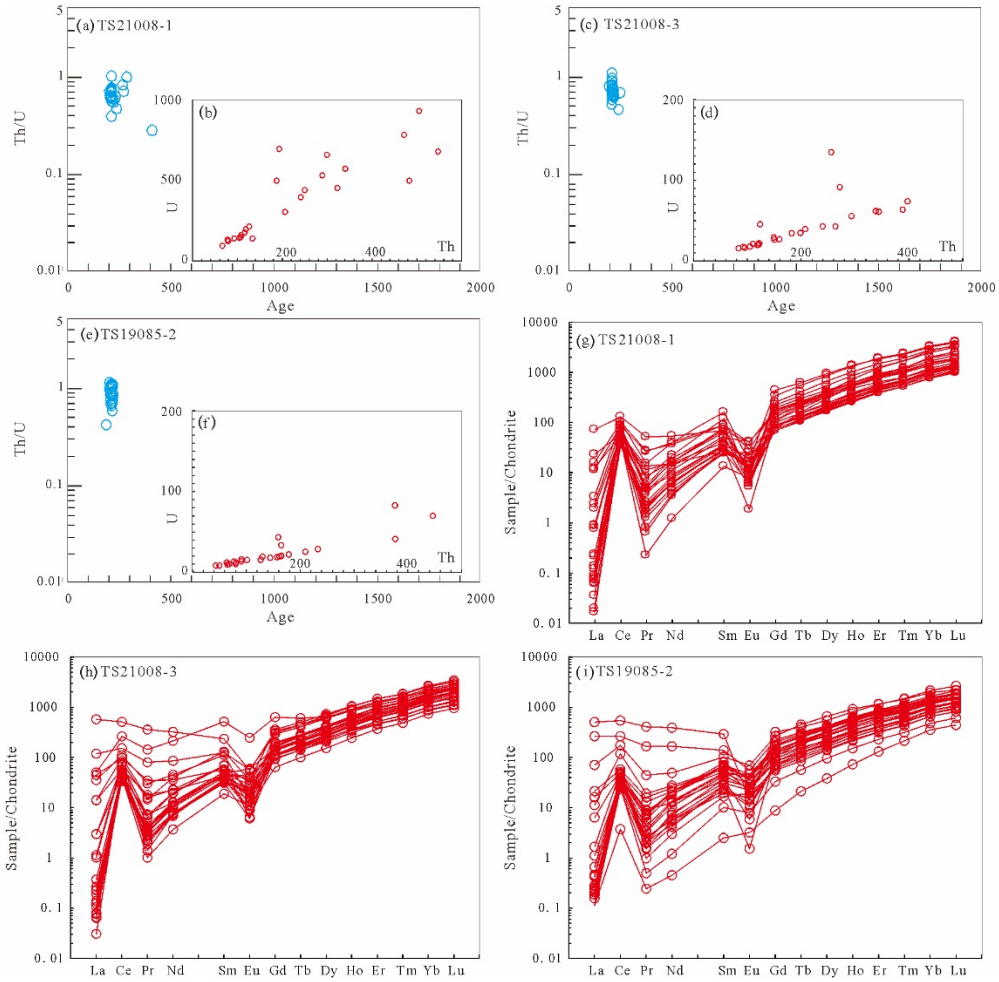

Figure 4. (a-f) Th/U-age and Th-U content of zircon; **(g-i)** Chondrite–normalized rare earth element (REE) patterns in the zircon grains.

The Th content of TS21008–3 zircon ranged from 83.50 × 10 ppm to 397.48 × 10 ppm, whereas the U content ranged from 131.61 × 10 ppm to 607.86 × 10 ppm. The Th/U ratio ranged between 0.44 and 4.06, and the majority of the Th/U ratios exceeded 0.4 (Figure 4c). The positive correlation between Th and U (Figure 4d) indicates the magmatic origin of zircon. The distribution pattern of rare earth elements demonstrates a left-leaning curve of heavy rare earth enrichment type, indicating negative Eu and positive Ce anomalies (Figure 4 h) (Supplementary Table S1). U-Pb isotope age analysis was performed on 25 zircons sampled from Banpo syenite porphyry, and 25 points were determined (Supplementary Table S2). After the exclusion of four data points with a harmony degree below 90%, the remaining $^{206}Pb/^{238}U$ age values ranged from 210 to 221 Ma. A majority of the zircon data points aligned with the harmony curve, while a few zircon data points deviated from the concordia. The possible reason for the deviation of data points can be attributed to the initial loss of common Pb in the zircon. However, this did not lead to a significant effect on the accuracy of $^{206}Pb/^{238}U$ age estimates. The weighted average age value of $^{206}Pb/^{238}U$ corresponds to 213.0 ±1.6 Ma, with MSWD = 0.92 (Figure 5c, d).

Preprints (www.preprints.org) | NOT PEER-REVIEWED | Posted: 10 November 2023 doi:10.20944/preprints202311.0705.v1

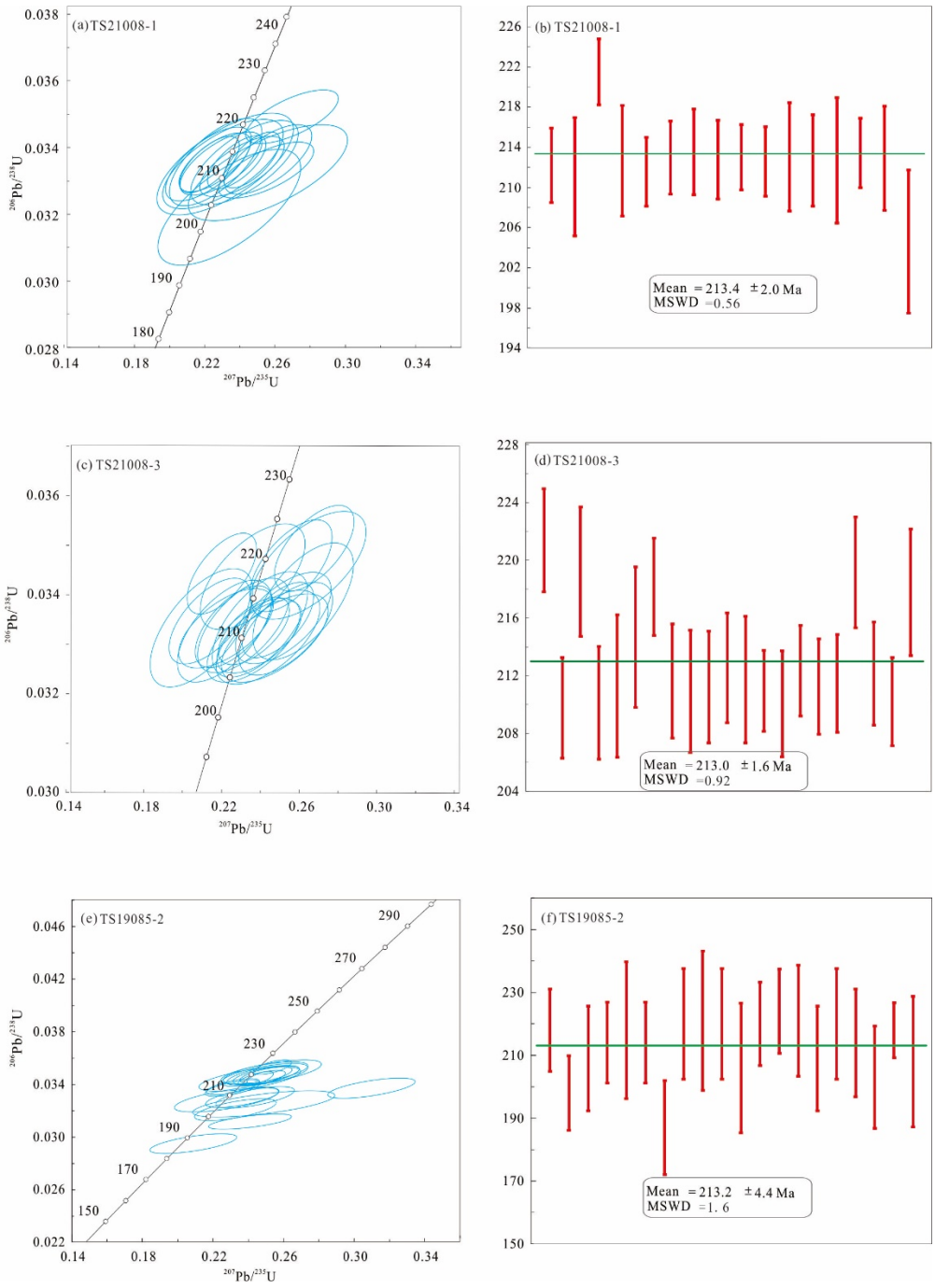

Figure 5. LA–ICP–MS zircon U–Pb concordia diagram and weighted average age diagram of zircons from Banpo Syenitic Porphyries in WNQOB.

The Th content of TS19085–2 zircon ranged between 58.20 × 10 ppm to 401 × 10 ppm, while the U content ranged between 58.82 × 10 ppm to 589.59 × 10 ppm. The Th/U ratio ranged between 0.41 and 1.11, and a majority of the Th/U ratios exceeded 0.4 (Figure 4e). The positive correlation between Th and U (Figure 4f) indicates the magmatic origin of zircon. The distribution pattern of rare earth elements demonstrates a left-leaning curve of heavy rare earth enrichment type, indicating negative Eu and positive Ce anomalies (Figure 4i) (Supplementary Table S1). U-Pb isotope age analysis was performed on 25 zircons sampled from Banpo syenite porphyry, and 25 points were determined (Supplementary Table S2). Among these, 20 zircons demonstrated good concordant values of $^{206}Pb/^{238}U$, and the remaining $^{206}Pb/^{238}U$ age values ranged between 203–224 Ma. A majority of the zircon data points aligned with the harmony curve. The weighted average age value of $^{206}Pb/^{238}U$ corresponds to 213.2 ±4.4 Ma, with MSWD = 1.6 (Figure 5e, f). All three age values were within the

Preprints (www.preprints.org) | NOT PEER-REVIEWED | Posted: 10 November 2023 doi:10.20944/preprints202311.0705.v1

acceptable error limit. Therefore, the crystallization ages of Banpo syenite porphyry were 213.4 ±2.1 Ma, 213.0 ±1.6 Ma, and 213.2 ±4.4 Ma, indicating the occurrence of the rock formation in the Late Triassic.

5.2. Whole-Rock Major and Trace Element Geochemistry

5.2.1. Characteristics of Major Elements

Significant variations were observed in the SiO_2 content of the syenite porphyry body, with three samples ranging from 55.21% to 58.43%, while the remaining samples ranged from 68.41% to 74.92%. The overall average value was 68.42%. In the TAS diagram (Figure 6a), most of the samples are located within the Intrusive rock region, certain samples are located within the trachyte dacite region, and three samples are located within the trachyte Andesite region. The K_2O content varied from 5.11% to 6.53%, while the Na_2O content varied from 2.83% to 4.20%. The alkali content was relatively high, with the alkalinity rate (AR) ranging from 2.11 to 4.81, and the $Na_2O + K_2O$ content ranging from 7.53% to 10.73%, with an average value of 9.41%. The K_2O/Na_2O ratio ranged from 1.30 to 2.24, indicating high potassium content and potassium-rich nature. The alkaline index (AI) varied from 0.60~0.88, indicating higher alkalinity. In the SiO_2-K_2O diagram (Figure 6b), a majority of the samples are located within the potassium region, with only 2 samples within the high potassium and calcium alkaline region. In the SiO_2-($Na_2O + K_2O$-CaO) diagram (Figure 6c), the samples are located within the alkaline region. The Al_2O_3 content varied from 13.44% to 17.58%, with an average of 15.42%. The aluminum saturation index, i.e., A/CNK value, was between 0.88 and 1.09, indicating a weakly peraluminous rock. In the A/NK-A/CNK diagram (Figure 6d), syenite porphyry is located within the peraluminous region, while Masanophyre is primarily located within the para-aluminous area.

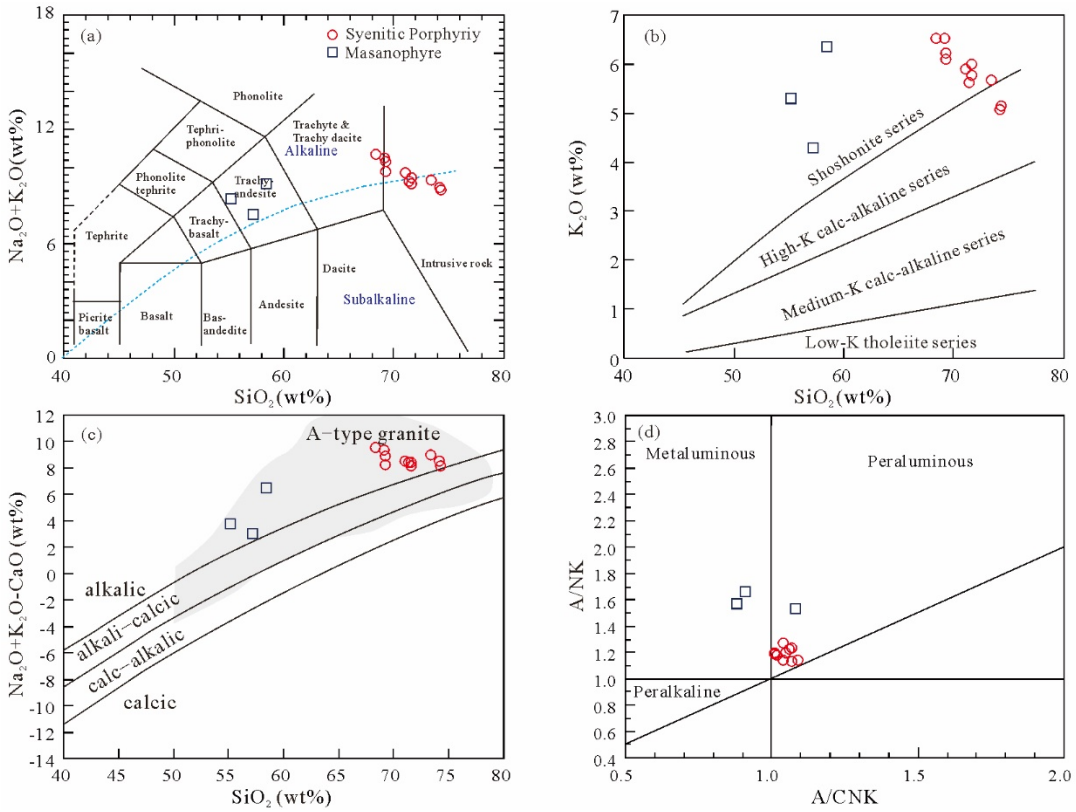

Figure 6. (**a**) TAS diagrams (after Middlemost [56]); (**b**) K_2O vs SiO_2 diagrams (after Rickwood [57]); (**c**) (Na_2O+K_2O-CaO)-SiO_2 diagrams (after Frost et al. [58]); (**d**) A/NK - A/CNK diagrams (after Maniar et al. [59]).

Preprints (www.preprints.org) | NOT PEER-REVIEWED | Posted: 10 November 2023 doi:10.20944/preprints202311.0705.v1

5.2.2. Characteristics of Trace Elements in the Whole Rock

A significantly high total rare earth elements (REE) content of the syenite porphyry was observed, with an ∑REE ranging from 142.89 ppm to 411.44 ppm and averaging 337.07 ppm (Supplementary Table S3). The region was strongly enriched with light rare earth elements (LREE), with ∑LREE ranging from 124.68 ppm to 390.40 ppm and averaging 316.37 ppm. As a result, the region was characterized by a significant loss of heavy rare earth elements (HREE), with ∑HREE ranging from 17.21 ppm to 26.31 ppm and averaging 20.70 ppm. The LREE/HREE ratio was 6.85–19.69. The $(La/Yb)_N$ ratio ranged from 7.47 to 29.83. Similarly, δEu ranged from 0.15 to 0.77, exhibiting a strong negative europium anomaly. The standardized partition curve of chondrite (Figure 7a) demonstrates a right dipping type with strong LREE enrichment, indicating the possible occurrence of garnet, rutile, and other minerals with strong enrichment of heavy rare earth elements in its source area.

The primitive mantle-normalized trace elements spider diagram are characterized by the enrichment of large ion lithophile elements such as Rb and La and the presence of high field strength elements such as Zr, Hf, and Pb (Figure 7b). On the contrary, certain elements, such as Ba, Sr, Nb, Ta, etc., demonstrated relative depletion.

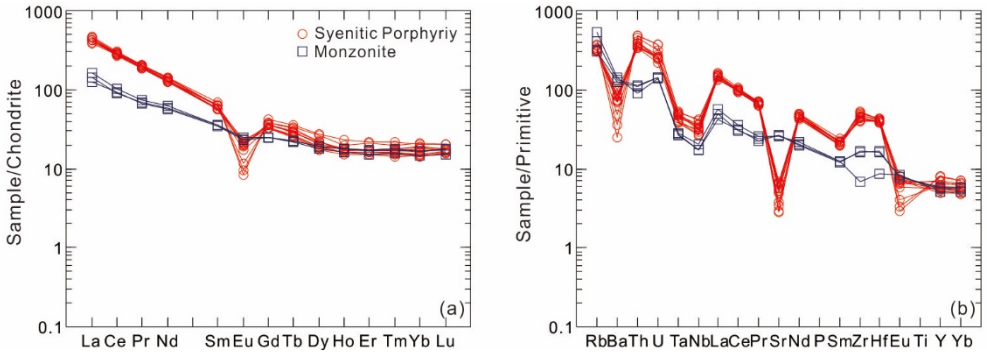

Figure 7. (**a**) Chondrite-normalized rare earth element (REE) patterns and primitive –normalized incompatible element distribution patterns for Banpo Syenitic Porphyries in WNQOB (chondrite data and primitive data for normalization taken from Sun and McDonough [60].

6. Discussion

6.1. Magma Source

Syenite is a type of alkaline rock representing post-collision, intraplate extension, or rift tectonic settings [38,39,61–63]. It can provide certain important information, such as the evolutionary relationship between continental lithosphere crust and mantle in the post-collision or intraplate tension settings. There are several perspectives on the origin of Syenite-like rocks. Some studies suggest that they are formed by a low degree of partial melting of heterogeneous lower crustal materials involving volatile matter or under high-pressure conditions [64,65]. Other studies propose partial melting of the enriched lithospheric mantle, which is a product of the crystallization differentiation of alkaline basaltic magma [66–68], and their formation by magma mixing, primarily because the mantle-derived mafic magma and crust-derived felsic magma undergo mixing to induce melting and further differentiation. Alternatively, they may be formed by the mixing of alkaline magma with mantle-derived silica unsaturated and crustal-derived granitic magma [69–71]. Presently, several scholars believe that the formation of Syenite-like rocks is mainly attributed to mantle source components [72,73].

The experimental petrology results also confirmed that syenite magma is related to mantle or mantle-derived materials. Based on the melting of experimental data from synthetic granite systems, i.e., the decrease in quartz content in the melt and the increase in albite content with the increase in pressure, Huang and Wyllie [64] speculated that the melting of continental crust rocks at the bottom of the thickened continental crust forms trachyte (syenite) rather than granitic magma. Further, Deng

 doi:10.20944/preprints202311.0705.v1

J F et al. [74] provided additional evidence to support this hypothesis from the perspective of rock phase equilibrium, referred to as high-pressure syenite , formed by partial melting of the crust with a pressure greater than 1.5 GPa, and inferred that it exhibits a rare earth distribution pattern without negative europium anomaly. Low pressure (P < 1.5Gpa) syenite is derived from the separation of plagioclase from basaltic magma and has evident negative europium anomaly [75]. However, the experiment by Litvinovsky et al. [76] demonstrated that the partial melting of felsic rocks under the condition of thickened crust does not produce syenitic magma; instead, it results in granitic magma. Similarly, the melting experiments conducted by metasomatic mantle rocks demonstrated the production of silicon-unsaturated nephelinite and other peralkaline rocks under high pressure. On the other hand, under low pressure, low melting can produce silicon-saturated trachyandesite and other potassic magma, and serve as the parent magma of potassic Syenite [77]. Long XP et al. [78] also obtained highly alkaline syenite (trachytic) melts through water loss melting of potassium-rich basaltic rocks (basaltic rocks) under high pressure. The petrology characteristics of the above rock experiments demonstrated that the melting of potassium-rich basic rocks or rich mantle rocks at the bottom of the thickened crust could form potassium-rich alkali syenitic magma or its parent magma. Conversely, the felsic rocks in the thickened continental crust cannot form syenitic magma, and as a result, the negative europium anomaly is not significant. Similarly, silicon-saturated Syenite formed by the melting in a low-pressure environment is derived from magma produced after the separation of plagioclase from basaltic magma, with significant negative europium anomaly.

6.2. Tectonic Setting

The genesis of the Banpo syenite porphyry can be compared to the genetic mechanisms involved in the formation of the Xiaohezi volcanic rocks and the Jinping quartz syenite porphyry in Yunnan [8,79–82], which were formed in a late collision strike-slip environment after the collision of the North China Block and the Yangtze Block. It was observed that a series of derived strike-slip pull-apart basins are often developed along the strike-slip faults. In system, several potassic alkali-rich igneous rocks also appeared, which are considered to be controlled by the intracontinental strike-slip transformation tectonic stress field [4,45,83]. The REE Chondrite of Banpo syenite porphyry exhibits a significant negative europium anomaly which is inconsistent with the experimental results of felsic matter melting to form syenite magma under controlled conditions. The rock mass also had a high SiO_2 content, with an average value of 68.42%, indicating that the silicon content had reached saturation. Thus, it can be inferred that the rock mass is unlikely to be a product of the partial melting of crustal material under crustal thickening conditions. Instead, it is a syenite magma formed by the melting in an extensional decompression environment, which is contaminated by crustal materials during ascending emplacement, leading to magma mixing with them. In addition, it is observed that the quartz syenite porphyry contains a certain amount of mafic enclave inclusions, revealing that the syenite porphyry intrusion is a product of mixing and further differentiation of syenite parental magma formed through the low melting of mantle-derived mafic magma at reduced pressure and crust-derived materials.

The unipolar photomicrographs of the syenite porphyry frequently demonstrated a banded structure of potassium feldspar surrounding quartz, indicating a large temperature difference in its formation. As a result of the mixing and solidification of magma, a potassium feldspar banded structure is formed surrounding the high-temperature quartz. Alkaline granite (A_1) in anorogenic environments within the plate exhibits a high Nb/Ta ratio (15.7–17.5) due to the addition of more mantle-derived or enriched mantle materials within the source area. The alkaline granite formed in post-collision environments (A_2 type, with a large amount of lower crust within the source area) exhibits a low Nb/Ta ratio, generally around 10–14 [84]. The Nb/Ta ratio of Banpo syenite porphyry varies from 11.20 to 14.49, with an average of 12.54. This shows a significant deviation from the Nb/Ta ratio of the original mantle, while the overall ratio is in agreement with that of the continental crust (Nb/Ta = 10 to 14 [84]), indicating the contamination of magma of Banpo syenite porphyry with the crustal materials during its ascent. The initial syenitic parent magma formed through the low partial melting of mantle-derived mafic magma at reduced pressure serves as a heat source for the melting

Preprints (www.preprints.org) | NOT PEER-REVIEWED | Posted: 10 November 2023 doi:10.20944/preprints202311.0705.v1

of lower crustal materials and undergoes mixing with them to a certain extent. Subsequently, it further crystallizes and differentiates to form Banpo syenite porphyry.

Numerous syenite types found globally are generally associated with A-type granite, indicating a certain relationship and common geochemical characteristics between the two in terms of genesis. Therefore, several scholars classified syenite as A-type granite. The high rare earth abundance, a seagull-type right dip partitioning curve, high alkali content, potassium-rich composition, and weakly peraluminous characteristics of the western Banpo syenite porphyry in the North Qinling orogenic belt are in agreement with the typical characteristics of A-type granite [35]. In the rock type discrimination diagram (Figure 8), all the rocks studied are classified within the A-type granite region. The zircon saturation temperature calculations for Banpo syenite porphyry also indicated its formation at higher temperatures (temperatures ranging from 706–907 °C, with an average temperature of 860 °C), which is consistent with the formation temperature of A-type granite higher than the formation temperatures of I-type and S-type granites. The average temperature of S-type granite is 764 ° C, while that of I-type granite is 781 °C [41]. In addition, its output strike-slip extensional environment aligns with the stress environment consistent with the extension of A-type granite output.

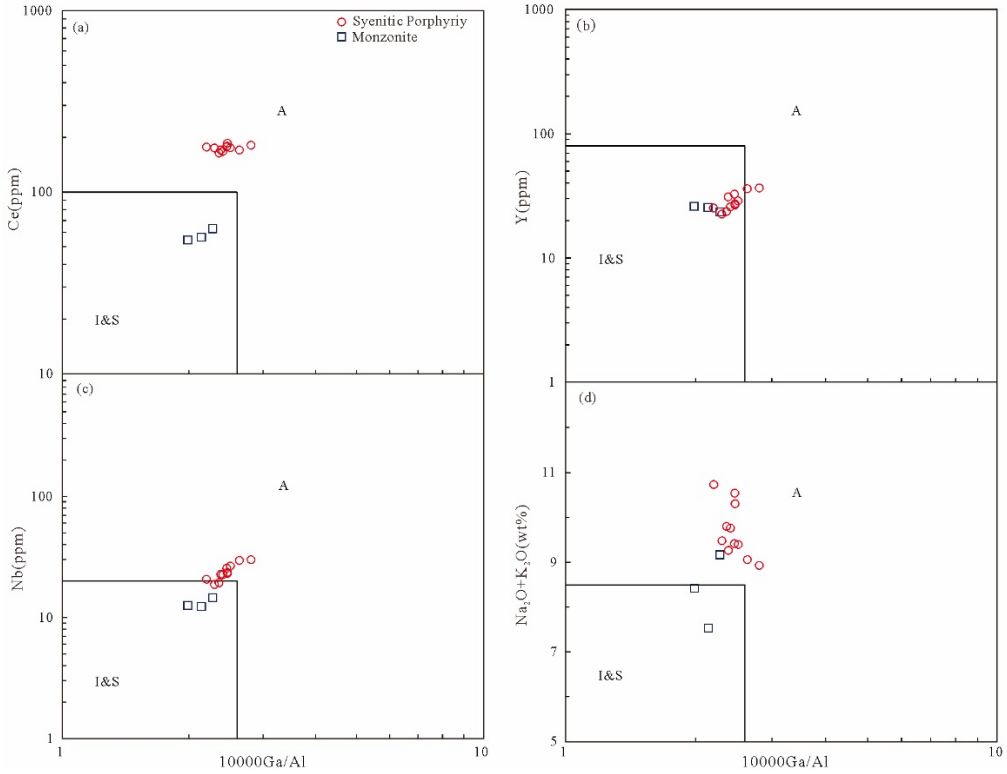

Figure 8. (**a**) (Na_2O + K_2O), (**b**)Nb, (**c**)MgO/K_2O and (**d**)((K_2O + Na_2O)/CaO) vs. 10,000Ga/Al discrimination diagrams for the Banpo Syenitic Porphyries in the WQOB (after Whalen et al. [36]). A = A-type granitoids; I = I-type granitoids; S = S-type granitoids.

During the Mesozoic, the most prominent feature at the Qinling-Qilian junction was the development of numerous 245–205 Ma-dominated granites of various types. There are diverse interpretations regarding the formation and tectonic background of these granites, such as synorogenic granite [85], post-collision granite [7,8,86], and anorogenic granite [87]. The statistical results of granite body formation ages indicated further differentiation into early Indosinian (243–233 Ma) and late Indosinian (220–205 Ma) [88]. The early Indo granites are generally characterized by the geochemical characteristics of island arc, and formed by the partial melting of the thickened lower crust formed through continental subduction or continental collision [46]. On the other hand, late Indosinian granites generally show the characteristics of post-collisional granites [19,89,90]. All the samples of Banpo syenite porphyry are located near collisional and intraplate granites on the tectonic

Preprints (www.preprints.org) | NOT PEER-REVIEWED | Posted: 10 November 2023 doi:10.20944/preprints202311.0705.v1

environment discrimination map (Figure 9a-b), indicating the intrusion formed in the post-collisional extension environment.

On the classification diagram of A-type granite subclasses Nb-Ce-Y and Nb-3Ga-Y (Figure 9c-d), all samples are positioned near the boundary between A1-type granite and A2-type granite, leaning toward the A1-type granite side. This suggests that they were formed during the transitional stage from post-orogenic to non-orogenic environments. Many experts believe that A-type granite is formed in an extensional environment [92–98] Considering the petrogenesis and regional characteristics, it is speculated that block continues to squeezes of the South China Block towards the North China Block and intraplate extension, the crust underwent partial melting to form the Banpo rock mass.

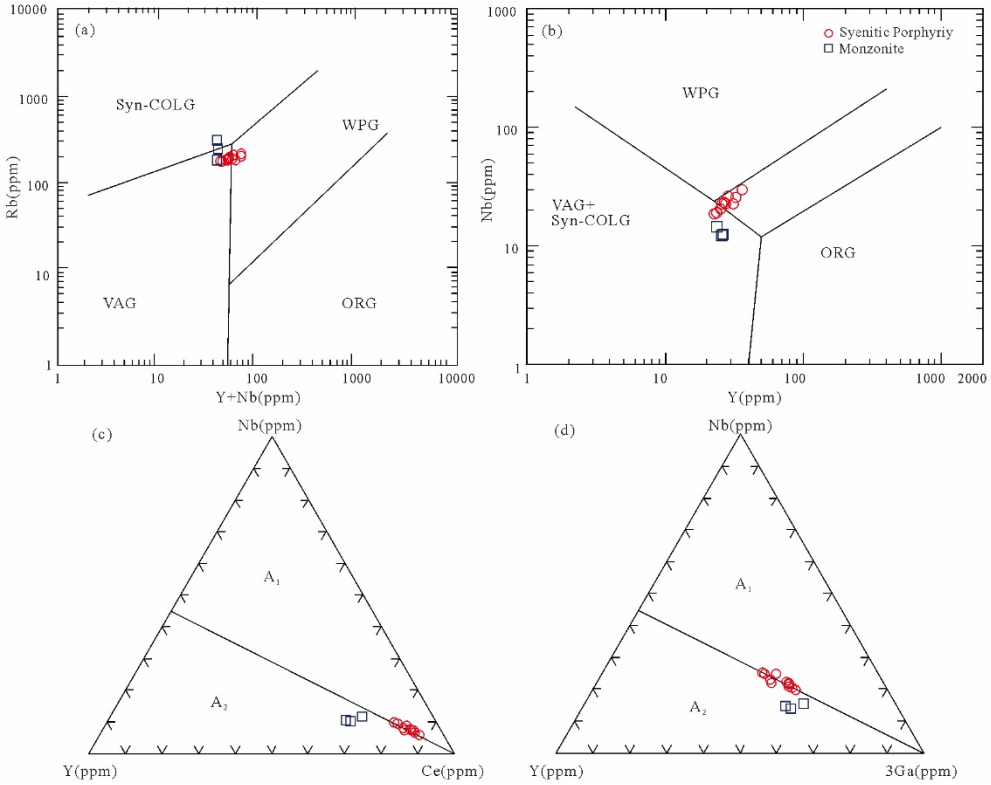

Figure 9. (**a**) Nb-Y diagrams; (**b**) Ta-Yb diagrams for the S Banpo Syenitic Porphyries the WNQOB (after Pearce et al. [91]); (**c**) Nb-Y-3Ga diagrams; (**d**) Nb-Y-Ce diagrams for the S Banpo Syenitic Porphyries the WNQOB (after Eby [38]). VAG =Volcanic arc granites; Syn-COLG = Syn-collision granites; WPG = Within-plate granites; ORG = Ocean ridge granites. A_1-type = anorogenic environment; A_2-type = post-orogenic environment.

6.3. Geological significance

Numerous studies have demonstrated that during the Indosinian period, collision orogeny occurred in the central orogenic system of North China, Qinling, and Yangtze Blocks. As a result, the Qinling Orogenic Belt transitioned into a typical intracontinental collisional orogeny during the Yangtze Block subducting beneath the Qinling micro-block along the Mianxian-Lueyang suture zone. This led to crustal thickening [26,99–105]. The thickened crust experienced significant heating and pressure, resulting in widespread melting and the development of various intermediate-acid intrusive rocks in the Qinling Orogenic Belt (from the west of the Henan Shaanxi border to the Tianshui area). The increased internal temperature of the crust caused partial melting of different types of rocks, leading to the formation of diverse types of granitic magma. Experimental petrology research indicates that at depths below 20 km under the crust, when the temperature reaches around 900 °C and water is present, Intrusive magma with strong upwelling capacity can be generated, either forming hypabyssal or ultra-hypabyssal granite bodies or erupting to the surface as rhyolite [75,106]. During collision orogeny, achieving such high temperatures of around 900 °C and partial melting in

the thickened lower crust is challenging unless there is an external heat supply from other sources [106]. The saturation temperature of zirconium in the Banpo syenite porphyry was calculated to obtain the magma crystallization temperature (ranging from 706 °C to 907 °C, with an average temperature of 860 °C). The commonly used formula for calculating Ti temperature in zircon is as follows: T（℃）=（5080±30）/［（6.01±0.03）-log（Ti）］-273[107]。 Such high temperatures are more likely to originate from mantle sources. After the completion of the collision orogeny in the Indosinian age, the North China Block and the Yangtze Block entered the lithosphere stretching stage, with mafic magma derived from the mantle intruding into the lower crust. This mafic magma provided heat for partial melting in the source area and contributed a small amount of mantle-derived material to the newly magma. This indicates that the eastern part of the North Qinling Orogenic Belt completed the primary collision orogeny during the late Indosinian period. Subsequently, the region underwent relaxation and gravity adjustments during the late orogenic period, transitioning into an extensional rifting phase in the post-orogenic stage. This phase is characterized by the formation of intermountain fault basins and pull-apart basins caused by block faulting, shear translation, and the occurrence of corresponding potassic alkali-rich igneous rocks.

7. Conclusions

(1) The LA-ICP-MS zircon U-Pb dating results indicate that the Banpo syenite porphyry in the western section of the North Qinling Orogenic Belt was formed during the Late Triassic, with ages of 213.4Ma ±2.1Ma (MSWD = 0.56), 213.0Ma ±1.6Ma (MSWD = 0.92), and 213.2Ma ±4.4Ma (MSWD = 1.6).

(2) The Banpo syenite porphyry in this region displays several characteristics, such as high rare earth abundance, a seagull-type right-dip partitioning curve, high alkali, and potassium content, and weakly peraluminous composition. These features are consistent with A-type granite, suggesting that it was formed during the transitional stage from post-orogenic to non-orogenic environments.

(3) During the late Late Triassic, the western section of the North Qinling Orogenic Belt experienced significant collision orogeny, which was followed by the intrusion of potassium-rich alkali intrusive rocks during subsequent orogenic stages.

Supplementary Materials: The following supporting information can be downloaded at: www.mdpi.com/xxx/s1,Table S1: Zircon trace element data of the Late Triassic orthophyre in the western part of the NQOB; Table S2: Zircon LA–ICP–MS U–Pb data of the Late Triassic orthophyre in the western part of the NQOB; Table S3: Whole-rock major and trace element data of the Late Triassic orthophyre in the western part of the NQOB.

Author Contributions: Conceptualization, S.L. and Z.L.; methodology, S.L. and X.P.; software, H.L., L.Q., S.J. and Y.Y.; validation, S.L., Z.L. and S.J.; formal analysis, S.L., Z.L. and H.L.; investigation,S.L., Z.L., X.P., H.L, L.Q., H.L., S.J. and J.R.; resources, S.L. and Z.L.; data curation, S.L. and Z.L.; writing—original draft preparation, S.L. and Z.L.; writing—review and editing, S.L., Z.L. and H.L.; visualization, S.L.; supervision, S.L. and Z.L; project administration, Z.L; funding acquisition, Z.L. All authors have read and agreed to the published version of the manuscript.

Funding: This research was funded by the National Nature Sciences Foundation of China (Grant Nos. 41872235, 42172236, 41872234, 41502191), Natural Science Basic Research Plan in Shaanxi Province of China (Grant Nos. 2019JM-312, 2019JQ-090, 2019JQ-209, 2020JM-229), the Fundamental Research Funds for the Central Universities (Grant Nos. 300102270202, 300103183081, 300103120009, 300104282717, 300102279204, 201810710233), China Scholarship Council (Grant No. 201806565026), and the Youth Innovation Team of Shaanxi Universities.

Data Availability Statement: The original contributions presented in the study are included in the article/Supplementary Material.

Acknowledgments: We thanks are extended to the chief editor and the two anonymous reviewers for their constructive reviews which have greatly improved our manuscript.

Conflicts of Interest: The authors declare no conflict of interest.

References

1. Zhang ,G.W.; Meng, Q.R;, Lai, S.C. Structures and Tectonics of the QinLing Orogenic belt.*Science in China*(Series B).**1995**, 25, 994–1003, (in Chinese).
2. Li, S.G.; Sun, W.D.; Zhang, G.W.; Chen, J.Y.; Yang. Y.C. Chronology and Geochemistry of HeiGouxia Metamorphic Volcanic Rocks in Mian-Lue Tectonic Belt, South Qinling:Evidence of the Paleozoic Ocean Basin and Its Closure age. *Science in China*(Series D).**1996**,03,223–230, (in Chinese).
3. Feng, Y.M.; Cao, X.D.; Zhang, E.P. Tectonic Evolution Framework and Nature of the West QinLing Orogenic Belt. *Northwestern Geology*.**2003**, 36(1), 1–10, (in Chinese with English abstract).
4. Pei, X.Z.; Ding, S.P.; Hu, B. Geochemical characteristics and tectonic significance of Cenozoic acid volcanic rocks in Tianshui area,West Qinling Mountains.*Acta Mineral. Sin.* **2004**(03), 227–235, (in Chinese with English abstract).
5. Dong, Y.P.; Zhang, X.N.; Liu, X.M.; Li, W.; Chen, Q.; Zhang, G.W.; Zhang, H.F.; Zhao, Y.; Sun, S.S.; Zhang, F.F. Propagation tectonics and multiple accretionary processes of the Qinling Orogen. *J. Asian Earth Sci*. **2015**, 104, 84–98.
6. Dong,Y.P.; Sun, S.S.; Santosh, M.; Hui, B.; Sun, J.P.; Zhang, F.F.; Cheng, B.; Yang, Z.; Shi, X.H.; He, D.F,et al. Cross Orogenic Belts in Central China: Implications for the tectonic and paleo geographic evolution of the East Asian continental collage. *Gondwana Res*. **2022**, 109, 18–88.
7. Zhang, H.F.;Jin, L.L.;Zhang,L,et al.Pb and Nd Isotopic Compositions of Basement and Granitoid in the Qilianshan : Constraints on Tectonic Affinity.*Earth Science*. **2006,** 01, 57–65, (in Chinese with English abstract).
8. Luo, B.J.; Zhang, H.F.;Xiao, Z.Q. Petrogenesis and tectonic implications of the Early Indosinian Meiwu Pluton in WestQinling,central China. *Earth Seience Frontiers* . **2012**, 19(3), 199–213, (in Chinese with English abstract).
9. Wang, X.X.; Wang, T.; Zhang, C.L. Neoproterozoic, Paleozoic, and Mesozoic granitoid magmatism in the Qinling Orogen, China: Constraints on orogenic process. *Journal of Asian Earth Sciences*. **2013**, 72, 129–151.
10. Huang, X.F.; Mo, X.X.; Yu, X.H.; Li, X.W.; Yang, M.C.; Luo, M.F.; He, W.Y.; Yu, J.C. Origin and geodynamic settings of the Indosinian highSr/Y granitoids in the West Qinling: An example from the Shehalijipluton in Tongren area. *Acta Petrologica Sinica.* **2014**,30 (11):3255 –3270, (in Chinese with English abstract).
11. Zhang, G.W.; Guo, A.L.; Yao, A.P. Qilian East Songpan Continental Tectonic Knot in Chinese Mainland.*Earth Seience Frontiers*. **2004**, 03, 23–32, (in Chinese with English abstract).
12. Zhao, D.H.; Ping ,X.Q.; Zheng,J.P.;Ai, L.; Deng, H. Geochemistry and Its Geological Significance of the Quartz Syenites in the Early Indosinian from the Tietang Gorge,West Qinling.*Earth Science*.**2019**,44(12),4203–4221, (in Chinese with English abstract).
13. Pei, X.Z.; Zhang, G.W.; Lai, S.C.; Li,Y.; Chen, L.; Gao, M. Main geological features of the Mianlue tectonic belt on the southern margin of the West Qinling. *Geological Bulietin of China***. 2002**, Z2, 486–494, (in Chinese with English abstract).
14. Dong, Y.P.; Zhang, G.W.; Neubauer F, Liu,X.M.; Genser, J.; Hauzenberger C. Tectonic evolution of the Qinling orogen，China: Reviewand synthesis. *Journal of Asian Earth Sciences*.**2011**,41 (3),213–237.
15. Dong, Y.P.; Sun, S.S.; Santosh, M.; Zhao, J.; Sun, J.P.; He, D.F.; Shi, X.H.; Hui, B.; Cheng, C.; Zhang, G.W. Central China Orogenic Belt and amalgamation of East Asian continents. Gondwana Res. 2021, 100, 131-194.
16. Huang, X.F.; Mo, X.X.; Yu, X.H,et al. Zircon U-Pb chronology,geochemistry of the Late Triassic acid volcanic rocks in Tanchang area,West Qinling and their geological significance. *Acta Petrologica Sinica*. **2013**, 29(11), 3968–3980, (in Chinese with English abstract).
17. Xu, X.Y; Wang H.L; Chen, J .L; Su, X. H; Wu, P; Gao, T. Zircon U-Pb age，element geochemistry of Mesozoicacid volcanic rocks at Yindaoshi area in westem Qinling. *ActaPetrologica Sinica*.**2007,**23(11),2845–2856, (in Chinese with English abstract).
18. Xu, X.Y.; Chen, J.L.; Gao, T,et al. Granitoid magmatism and tectonic evolution in northern edge of the Western Qinling terrane,NW China. *Acta Petrologica Sinica*. **2014**, 30(2), 371 -389, (in Chinese with English abstract).
19. Wang, X.X.; Wang, T. Zhang, C.L. Granioid magmatism in the Qinling orogen, central China and its bearing on orogenic evolution. Science China:*Earth Sciences*. **2015**, 58: 1497–1512, doi: 10.1007/s11430-015–5150-2, (in Chinese).
20. Li, X.W.; Mo, X.X.; Huang, X.F.; Dong, G.C.; Yu, X.H.; Luo, M.F.; Liu, Y.B. U-Pb zircon geochronology,geochemical and Sr-Nd-Hfisotopic compositions of the Early Indosinian 'Tongren pluton in WestQinling: Petrogenesis and geodynamic implications. *Journal of Asian Earth Sciences*. **2015**, 97: 38-50.

21. Qiu, K.F.; Yu, H.C.; Gou, Z.Y.; Liang, Z.L.; Zhang, J.L.; Zhu, R. Nature and origin of 'Triassic igneous activity in the Western Qinling Orogen: The Wenquan composite plutonexample. *International Geology Review* . **2018**, 60(2): 242–266.
22. Xiong, X.; Zhu, L.M.; Zhang, G.W.; Santosh M.; Jiang, H.; Zheng, J.; Guo, A.L.; Ding, L.L. Petrogenesis and tectonic implications ofIndosinian granitoids from Western Qinling Orogen,China: Productsof magma-mixing and fractionation. *Geoscience Frontiers*. **2020**,11 (4) :1305–1321.
23. Xing, H.Q.; Li, X.W.; Xu, J.F.; Mo, X.X.; Shan, W.; Yu, H.X.; Hu, J.Q.; Huang, X.F.; Dong, G.C. The genesis of felsic magmatism during theclosure of the northeastern Paleo-Tethys Ocean: Evidence from the Heri batholith in West Qinling,*China. Gondwana Research*. **2020**,84: 38–51.
24. Yin, A.; Nie, S.Y. An indentation model for the North and South China collision and the development of the Tan-Lu and Honam faultsystems ,eastern Asia. *Tectonics*. **1993**,12(4),801–813.
25. Lu, X.X.; Dong, Y.; Chang, Q.L.; Xiao, Q.H.; Li, X.B.; Wang, X.X. Qinling Indosinian Shahewan Ordovician rapakivi granite and its dynamic significance.*China(Series D)*. **1996**, 03, 244–248, (in Chinese).
26. Zhang, B.R. Tectonic-Geochemistry district and orogenic movement model in Qinling Mountains.State Key Laboratory of Mineralization Research, Department of Earth Sciences, *Nanjing University*. **2002**:4, (in Chinese with English abstract).
27. Wang, X.X.; Wang, T.; Jahn,B. M.;Hu, N.G.; Chen, W. Tectonic significance of Late Triassic post-collisional lamprophyre dykes from the Qinling Mountains (China). *Geological Magazine*. **2007**, 144, 837–848.
28. Chen, Y.J.; Santosh, M. Triassic tectonics and mineral systems in the Qinling Orogen, central China. *Geological Journal*. **2014**, 49, 338–358.
29. Li, X.F.; Li, Y.S.; Dong, G.C.; Li, X,et al. Granitoid magmatism and tectonic evolution in the eastern part of the West Qinling;Constraints from geochemistry , zircon U-Pb chronology and Hf isotopic.*Acta Petrologiea Siniea.* **2021**, 37(6),1691–1712, (in Chinese with English abstract).
30. Qian, Z.S.; Yang, F.; Chao, L.; Xue, F.; Santosh, M.; Yang, B.; Zhang, S.; Sung Won Kim. Late Mesozoic Huang beiling S-type granite in the East Qinling Orogen, China: Geochronology, petrogenesis and implications for tectonic evolution. *Geochemistry*. Volume 82, Issue 1, (4) **2022**, 125857.
31. Li, X.; Dong, G.; Yu, X.; Li, Y.; Santosh, M.; Lv, X,et al. Evidence for magma mixing during triassic magmatism in west Qinling, china: constraints from petrology, geochemistry, U-Pb zircon geochronology, and Sr-Nd-Hf isotopic of the baguashan pluton. *Geological Journal*. **2021**.
32. Bai, B.W.; Chen, D.L.; Zhu, X.H.; Ren, Y.F.; Luo, F.H.; Wang, H.J. A-type granite and dark enclaves in the North Qinling Orogenic Belt: Constrains on the tectonic affinity between the North Qinling Orogenic Belt and the North China Craton. *Precambrian Research*. **2021**, 357,106-117.
33. Ma, J.; Lü, X.B.; Li, S.; Chen, J.J.; Lu F.; Yin, X.; Wu, M.Q. The ca. 230 ma gold mineralization in the fengtai basin, western Qinling orogen, and its implications for ore genesis and geodynamic setting: a case study of the matigou gold deposit. *Ore Geology Reviews*.**2021**.
34. Loiselle, M.C.; Wones, D.R. Characteristics and origin of anorogenic granites. *Geol. Soc. Am. Abstr. Prog*. **1979**, 11, 468.
35. Collins,W.J.; Beams,S.; White, A.J.R.; Chappell, B.W. Nature and origin of A-type granites with particular reference to southeastern Australia. *Contributions to Mineralogy Petrology*. **1982**, 80, 189–200.
36. Whalen, J.B.; Currie, K.L.; Chappell, B.W. A-type granites: Geochemical characteristics, discrimination and petrogenesis. *Contrib. Mineral. Petrol.* **1987**, 95, 407–419.
37. Eby, G.N. The A-type granitoids: A review of their occurrence and chemical characteristics and speculations on their petrogenesis. *Lithos*. **1990**, 26, 115–134.
38. Eby, G.N. Chemical subdivision of the A-type granitoids: petrogenetic and tectonic implications. *Geology*. **1992**, 20(7): 641–644.
39. Bonin, B. From orogenic to anorogenic settings: Evolution of granitoid suites after a major orogenesis. *Geological Journal*. **1990**, 25, 261-270.
40. Bonin, B. A-type granites and related rocks: Evolution of a concept, problems and prospects. *Lithos.* **2007**, 97, 1–29.
41. King, P.L.; White, A.J.R.; Chappell, B.W.; Allen, C.M. Characterization and Origin of Aluminous A-type Granites from the Lachlan Fold Belt, Southeastern Australia. *Journal of Petrology*. **1997**, 38, 371-391.
42. Mushkin, O.; Navon, L.; Halicz, G. Hartmann .; M. Stein. The Petrogenesis of A-type Magmas from the Amram Massif, Southern Israel. *Journal of Petrology*. **2003**, 44, 815–832.
43. Xiao, E.; Qiu, J.S.; Xu, X.S.; Jiang, S.Y.; Hu, J.; Li, Z. Chronology, geochemistry, petrogenesis and tectonic implications of Yaokeng Alkaline granites in Zhejiang Province. *Acta Petrol. Sin.* **2007**, 23, 1431–1440, (In Chinese with English abstract).

44. Abuduxun, N.; Windley, B.F.; Xiao, W,et al. Carboniferous tectonic incorporation of a Devonian seamount and oceanic crust into the South Tianshan accretionary orogen in the southern Altaids. *International Journal of Earth Sciences*. **2021**:1–19.
45. Zhang, G.W.; Dong, Y.P.; Yao, A.P. Review on the development of studies on the tectonic and orogen process of orogenic belt,and discussing on some new key problems.*NorthWest Geology*. **2001**, 34(1):1–9, (in Chinese with English abstract).
46. Xu, X.Y.; Chen, J.L.; Yan, Z.; Wang, R.T.; Li, P.; Li, T.; Wang, H.L.; Yang, Y.Z.; Yang, J.L.; Li, Z.P.; Ma, Z.P.; Zhu, T.; Tang, Z.; Zhang, Y.; Sun, J.M.; Zhu, X.H. Geological Map (1:500000) of Qinling and Adjacent Areas. *Xi'an: Xi'an Map Publishing House*, **2014**, (In Chinese with English Abstract)
47. Liu,Y.S.,Zong,K.Q.,Kelemen,P.B.,et al.,2008.Geochem‐ istry and Magmatic History of Eclogites and Ultramafic Rocks from the Chinese Continental Scientific Drill Hole: Subduction and Ultrahigh ‐ Pressure Metamorphism of Lower Crustal Cumulates.Chemical Geology,247(1-2): 133-153. https://doi. org/10.1016/j. chem‐ geo.2007.10.016.
48. Liu,Y.,Gao,S.,Hu,Z.,et al.,2010.Continental and Oceanic Crust Recycling ‐ Induced Melt ‐ Peridotite Interactions in the Trans ‐ North China Orogen: U ‐ Pb Dating, Hf Iso‐ topes and Trace Elements in Zircons from Mantle Xeno ‐ liths. Journal of Petrology, 51(1-2): 537-571. https:// doi.org/10.1093/petrology/egp08.
49. Liu, Y.S.; Hu, Z.C.; Zong, K.Q.; Gao, C.G.; Gao, S.; Xu, J.; Chen, H.H. Reappraisement and refinement of zircon U-Pb isotope and trace element analyses by LA-ICP-MS. Chin. Sci. Bull. 2010, 55, 1535–1546.
50. Ludwig, K. User's manual for isoplot 3.00: a geochronological toolkit for microsoft Excel.Berkeley: Berkeley Geochronology Center, 2003:25-32.
51. Li, H.K.; Geng, J.Z.; Zhang, Y.Q.; Li, H.Q. Using Laser Ablation Multi Receiver Plasma Mass Spectrometer Study on the Determination of U-Pb Isotopic Age of Zircon by LA-MC-ICPMS.Acta Mineralogica Sinica.2009, 29S1, 600–601, (in Chinese with English abstract).
52. Ma,Q.,Zheng,J.P.,Griffin,W.L.,et al.,2012.Triassic"Ada ‐ kitic"Rocks in an Extensional Setting (North China): Melts from the Cratonic Lower Crust. Lithos, 149(15): 159-173.https://doi.org/10.1016/j.lithos.2012.04.017.
53. Belousova,E.A.; Griffin, W. L.; O'Reilly, S.Y.; Fisher N.I. Igneous zircon: trace element composition as an indicator of source rock type. Contributions to Mineralogy Petrology. 2002, 143, 602-622.
54. Wu, Y.B.; Zheng, Y.F. Genesis of zircon and its constraints on interpretation of U-Pb age. Chinese Science Bulletin. 2004, 49, 1554–1569.
55. Siebel, W.; Blaha, U.; Chen, F.; Rohrmüller, J. Geochronology and geochemistry of a dyke–host rock association and implications for the formation of the Bavarian Pfahl shear zone, Bohemian Massif. International Journal of Earth Sciences. 2005, 94, 8-23.
56. Middlemost, E.A.K. Naming materials in the magma/igneous rock system. Earth-Sci. Rev. 1994, 37, 215–224.
57. Rickwood, P.C. Boundary lines within petrologic diagrams which use oxides of major and minor elements. Lithos. 1989, 22, 247-263.
58. Frost, C.D.; Frost, B.R. On ferroan (A-type) granitoids: their compositional variability and modes of origin. J. Petrol. 2010, 52, 39–53.
59. Maniar, P.D.; Piccoli, P.M. Tectonic discrimination of granitoids. Geol. Soc. Am. Bull. 1989, 101, 635–643.
60. Sun, S.S.; Mcdonough, W.F. Chemical and isotopic systematics of oceanic basalts: Implications for mantle composition and processes. Geol. Soc. Lond. Spec. Publ. 1989, 42, 313-345
61. Whalen J B, Currie K L, Chappell B W. A-type granites: geochemical characteristics, discrimination and petrogenesis.Contributions to mineralogy and petrology .1987, 95: 407–419.
62. Sylvester, P.J. Post-collisional strongly peraluminous granites. lithos. 1998,45(1/4):29-4.
63. Bonin, B.; Sekkal, A.A.; Bussy, F,et al.Alkali-calcic and alkaline post-orogenic granite magmatism:petrologic constraints and geodynamic settings.Lithos. 1998, 45,45–70.
64. Huang, W.L.; Wyllie, P.J. Phase relationships of S-type granite with H2O to 35 kbar: muscovite granite from Harney Peak, South Dakota. J. Geophys. Res. 1981,86, 10515-10529.
65. Lubala, R.T.; Frick, C.; Roders, J.H.; Walraven, F. Petro-genesis of syenites and granites of the Schiel Alkaline complex,Northern Transvaal, South Africa. J. Geol. 1994,102, 307–309.
66. Brown, P.E.; Becker, S.M. Fractionation, hybridisation and magma-mixing in the Kialineq centre East Greenland. Contrib.Mineral. Petrol. 1986,92, 57-70.
67. Lynch, D.J.; Musselman, T.E.; Gutmann, J.T,et al. Isotopic evidence for the origin of Cenozoic volcanic rocks in the Pinacate volcanic field,northwestern Mexico[J].Lithos.1993,29(3-4), 295–302.

68. Yang, J.H.; Chung, S.L.; Simon, A. Wilde, Wu, F.Y.; Chu, M.F.; Lo, C.H.; Fan, H.R. Petrogenesis of post-orogenic syenites in the Sulu Orogenic Belt, East China: geochronological, geochemical and Nd–Sr isotopic evidence. Chemical Geology. 2005, 214, 99–125.
69. Dorais, M.J. Compositional variations in pyroxenes and amphiboles of the Belknap Mountain complex, New Hamp-shire: evidence for origin of silica-saturated alkaline rocks.Am. Mineral. 1990,75, 1092- 1105.
70. Litvinovsky, B.A.; Jahn, B.M.; Zanvilevich, A.N.; Shadaev, M.G. Crystal fractionation in the petrogenesis of an alkali monzodiorite-syenite series: the Oshurkovo plutonic sheeted complex, Transbaikalia, Russia. Lithos. 2002,64, 97–130.21.
71. Qin, J.F.; Lai, S.C.; Grapes, R.; Diwu, C.R.; Ju, Y.J.; Li, Y.F. Origin of Late Triassic high-Mgadakitic granitoid rocks from the Dongjiangkou area,Qinling orogen,Central China implications forsubduction of continental crust. Lithos. 2010,120(3-4),347-367.
72. Stern, R. J . Subduction zones . Reviews of Geophysics,◎2002, 40 （4） ,1012◎doi:10.1029 / 2001RG000108.
73. Zhang, H.R.; Hou, Z.Q.; Yang, T.N,et al. Subduction-related Quartz. Syenite Porphyries in the Eastern Qiangtang Terrane,Qinghai-Tibet Plateau:Constraints from geochemical analyses.Geological review,2010,56(03):405–414, (in Chinese with English abstract).
74. Deng, J.F.; Zhao, H.L.; Luo, Z.H.; Guo, Z.F.; Mo, X.X. Mantle plumes and lithosphere motion in East Asia. In: Flower MFJ, Chung SL, Lo CH, Lee TY (eds.). Mantle Dynamics and Plate Interactions in East Asia. Washington DC: American Geophysical Union. 1998, 59–65.
75. Deng, J.F.; Qiu, R.Z.; Xiao, Q.H,et al. Input of Material and Heat from Convective Mantle into Continent and Continental Metallogenesis.Mineral Deposits. 2004, 23(S1):24-31, (in Chinese with English abstract).
76. Litvinovsky, B. A.; Steele, I.M.; Wickham, S.M. Silicic magma formation in overthickened crust:melting of charnockite and leucogranite at 15,20 and 25 kbar. Journal of Petrology. 2000,41(5):717–737.
77. Xiao, Q.H.; Deng, J.F.; Qiu,R.Z,et al. A preliminary study of the relationship between granitoids and the growth of continental crust: a case study of the formation of key orogen granitoids in China.Geology in China. 2009, 36(03), 594-622, (in Chinese with English abstract).
78. Long, X.P.; Sun, M.; Yuan, C.; Xiao, W.J.; Lin, S.F.; Wu, F.Y.; Xia, X.P.; Cai, K.D. Detrital zircon age and Hf isotopic studies for meta sedimentary rocks from the Chinese Altai:Implications for the Early Paleozoic tectonic evolution of the Central Asian Orogenic Belt.Tectonics. 2007, 26,TC5015.doi:101029/2007TC002128.
79. Pei, X.Z.; Li, Z.C.; Ding, S.P,et al. Geochemical characteristics and zircon U- Pb ages of island- arc basic igneous complexes in the Tianshui area,West Qinling. Geology of China, 2005,04, 5–16, (in Chinese with English abstract).
80. Ding, S.P.; Pei, X.Z.; Hu, B,et al.Geochemical Characteristics and Origin of Cenozoic Acid Volanic Rocks In the TianShui area Gansu province.Geology and Prospecting. 2005,01, 33-37, (in Chinese with English abstract).
81. Xu, L.L.; Bi, X.W.; Su, W.C,et al. Geochemical characteristis andpetrogenesis of the quartz syenite porphyry from Tongchang porphyry Cu(Mo-Au) deposit in Jinping County,Yunan Province. Acta Petrologica Sinica. 2011, 27 (10), 3109–3122.
82. Li, L.; Meng, Q.R.; Pullen, A.; Garzione, C.N.; Wu, G.L.; Wang, Y.L.; Ma, S.X.; Duan, L. Late Permian-Early Middle Triassic back-arcbasin development in West Qinling,China. Journal of Asian EarthSciences. 2014, 87, 116–129.
83. Hou, Z.Q.; Qu, X.M.; Yang, Z.S,et al.Metallogenesis in Tibetan collisional orogenic belt:III.Mineralization in post-collisional extension setting.Mineral Deposits. 2006,06, 629–651, (in Chinese with English abstract).
84. Zhao, Z.H.; Xiong,X.L.; Wang, Q,et al. Some aspects on geochemistry of Nb and Ta.Geochemistry. 2019, 44(12), 4203-4221, (in Chinese with English abstract).
85. Sun, W.; Li, S.; Chen, Y .; Li, Y. Timing of synorogenic granitoids in the south Qinling, central China: constraints on the evolution of the Qinling-Dabie orogenic belt. J. Geol. 2002,110,457–468.
86. Zhang, C.L.; Wang, T.; Wang, X.X. Genesis and tectonic setting of early Mesozoic granites in the Qinling Orogenic belt.Geological Journal of China Universities. 2008, 53(03), 304-316, (in Chinese with English abstract).
87. Ji, S.; Li, Z.C.; Pei, X.Z.; Pei, L.; Li, R.B.; Liu, C.J.; Chen, Y.X.; Lin, H.; Wang, M. Petrogenesis and Tectonic Significance of Late Triassic A1-Type Granite from the West Section of North Qinling Orogenic Belt: Constraints from Geochronology and Geochemistry. Minerals. 2023 , 13(4), 557.
88. Gong, X.K.; Chen, D.L.; Zhu, X.H.; Dong, Z.C.; Guo, C.L. The determination of Triassic ultramafic-syenite intrusive body and its geological signifcance, western North Qinling. Acta Petrologica Sinica. 2016,32(1),177–192,(in Chinese with English abstract).
89. Zhu, L.M.; Ding, Z.J.; Yao, S.Z,et al. Metallogenic Geological Events and Metallogenic Tectonic Background of the Wenquan Molybdenum Deposit in Gansu, West Qinling Mountains.Science Bulletin.2009, 54(16),2337-2347+2439-2441,(in Chinese).

90. Li, Z.C.; Pei, X.Z.; Li, R.B.; Pei, L.; Hu, B.; Liu, C.J.; Chen, G.C.; Chen, Y.X. LA-ICP-MS zircon U-Pb dating, geochemistry of the Mishuling intrusion in western Qinling and their tectonic significance. Acta Petrologica Sinica. 2013,29(8) , 2617-2634, (in Chinese with English abstract).
91. Pearce, J.A.; Harris, N.; Tindle, A.G. Trace Element Discrimination Diagrams for the Tectonic Interpretation of Granitic Rocks. J. Petrol. 1984, 25, 956–983.
92. Clemens, J.D.; Holloway, J.R.; White, A.J.R. Origin of an A-type granite: experimental constraints. American Mineralogist. 1986, 71, 317–324.
93. Whalen, J.B.; Currie, K. L.; Chappell, B.W. A-type granites: geochemical characteristics, discrimination and petrogenesis. Contributions to Mineralogy Petrology. 1987, 95, 407-419.
94. Maniar, P.D.; Piccoli, P. M. Tectonic discrimination of granitoids. Geological Society of America Bulletin. 1989, 101, 635–643.
95. Hong, D.W.; Wang, S.G.; Han, B.F,et al. Classification and identification criteria of tectonic environment of alkaline granite.Science China(Series B). 1995, 04, 418-426, (in Chinese).
96. Douce, A.E.P. Generation of metaluminous A-type granites by low-pressure melting of calc-alkaline granitoids. Geology. 1997, 25, 743–746.
97. Dall'Agnol, R.; Frost, C.D.; Rämö, O.T. A-Type Granites and Related Rocks Through Time. Geochimica et Cosmochimica Acta. 2005, 69.
98. Jia, X.H.; Wang, Q.; Tan, G.J. A-type Granites:Research Progress and Implications.Geotectonica et Metallogenia. 2009, 33, 465-480, (in Chinese with English abstract).
99. Zhang, B.R. Magmatic Activity from source in the Qinling Orogenic belt and Its Dynamic Significance.Earth Science Frontiers. 2001, 03, 57–66, (in Chinese with English abstract).
100. Zhou, W.G.; Zhang, B.R.; Yang, W.R,et al. Geochemical characteristics and tectonic Implications of post collision intermediate acid volcanic rocks from Qinling Dabie Orogen.Geochemistry. 1998, 06, 537-548, (in Chinese with English abstract).
101. Zhang, H.F.; Luo, T.C.; Zhang, B.R. The Source Characteristics and Tectonic Environment of the Piaochi batholith in the North Qinling.Geological Review. 1996, 03, 209–214, (in Chinese with English abstract).
102. Zhang, H.F, Ouyang, J.P.; Lin, W.L. Pb,Sr,Nd Isotope Composition of Ningshan Granitoids,South Qinling and their Deep Geological Information.Journal of Mineralogy.1997,01,23-26+28–33, (in Chinese with English abstract).
103. Jiang, Y.H.; Jin, G.D.; Liao, S.Y.; Zhou, Q.; Zhao, P . Geochemical and Sr–Nd–Hf isotopic constraints on the origin of Late Triassic granitoids from the Qinling orogen, central China: Implications for a continental arc to continent–continent collision. Lithos. 2010, 117, 183-197.
104. Dong, Y.P.; Zhang, G.W.; Neubauer, F.; Liu, X.M.; Genser,J.; Hauzenberger, C. Tectonic evolution of the Qinling orogen, China: Review and synthesis. Journal of Asian Earth Sciences. 2011, 41, 213–237.
105. Kong, J.J.; Niu, Y.L.; Duan, M,et al. Petrogenesis of Luchubaand Wuchaba granitoids in western Qinling: Geochronological andgeochemical evidence. Mineralogy and Petrology .2017, 111(6), 887–908.
106. Patino Douce, A.E.; Harris, N. Experimental constraints on Himalaya anatexis .Journal of Petology. 1998, 39, 689–710.
107. Watson E B，Harrison T M . Zircon thermometer reveals minimum melting conditions on earliest Earth [J] . Science，2005，308：841-844 .